

pubs.acs.org/JPCC Article

Effects of Proaromaticity on Excited-State Lifetimes and Charge Separation in Near-Infrared Sensitizer Dyes in Solution and on TiO₂

Austin L. Dorris, Jonathon Watson, Jacquelyn J. Mosely, Ethan C. Lambert, Gregory S. Tschumper,* Jared H. Delcamp,* and Nathan I. Hammer*



Cite This: J. Phys. Chem. C 2023, 127, 649–659



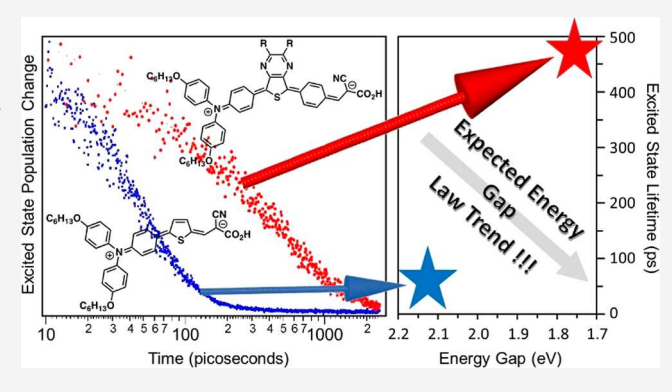
ACCESS I

III Metrics & More

Article Recommendations

s Supporting Information

ABSTRACT: The influence of proaromaticity on the excited state dynamics of near-infrared (NIR)-absorbing sensitizer dyes is explored using a combination of ultrafast transient absorption spectroscopy (TAS) and computational chemistry. The addition of a proaromatic π -bridge was found to stabilize the excited state and lead to lower excitation energies in solution and longer excited-state lifetimes, contrary to what is expected by the energy gap law. When studied under standard device conditions on TiO_2 , it was found that the dye structure plays a significant role in determining excited-state dynamics. Computational chemistry results confirm the proaromatic nature of the dyes through both bond length analyses and nucleus-independent chemical shift (NICS) calculations. Through incorporation of excited-state aromaticity, a $10\times$



increase in excited-state lifetime was observed for dyes with a near 0.5 V lower energy excited state.

■ INTRODUCTION

Increasing the excited-state lifetime of molecular materials is an active area of research with wide-reaching applications such as with photodetectors, 1-3 dye-sensitized photoelectrochemical cells (DS-PECs),⁴⁻⁶ organic photovoltaics,^{7,8} non-linear optical materials, emissive materials, and with dye-sensitized solar cells (DSCs). 11 In particular, molecular optical materials with narrow optical band gaps are intriguing to study due to the energy gap law reducing excited-state lifetimes at longer wavelengths. $^{10,12-16}$ The energy gap law generally predicts that as molecular systems absorb longer wavelengths of light, the excited-state lifetimes tend to decrease due to increasing nonradiative relaxation pathway rates. The rapid excited-state decay of near-infrared (NIR) absorbing dyes competes with photoinduced interfacial electron transfer reactions in solar cells (such as with DSC and DS-PEC systems), which makes high power conversion efficiencies at lower energy wavelengths more difficult to achieve. 11,17 Strategies that extend the excitedstate lifetime and charge separation duration across interfaces with molecular systems are exceptionally important to a range of technologies. Herein, we probe the effects of dyes incorporating proaromaticity on excited-state kinetics in solution and charge separation lifetimes on a metal oxide semiconductor surface (TiO₂).

Metal oxide-anchoring dyes are important to DS-PEC and DSC systems. ¹¹ These systems typically operate through photoexcitation of a dye followed by injection of electrons into the conduction band of a semiconducting metal oxide such as

 ${
m TiO_2}$. One of the biggest challenges in designing dyes for ${
m TiO_2}$ -based systems is incorporating chromophores that cover not only the ultraviolet and visible spectrum but also the NIR as well. $^{17-20}$

Optimizing the optical and physical properties of organic dyes has seen an explosion of activity since the report of the modern form of DSCs in 1991. Organic dyes have emerged as an attractive option that use non-precious metals and give the highest performances in DSCs. An emerging trend is that dyes, which incorporate donor (D), π -bridge, and acceptor (A) components, have proven to be some of the more successful organic dyes in recent years. Carefully engineered D- π -A molecules that facilitate the efficient transfer of charge also offer the added benefit of tunability into the NIR region of the solar spectrum. This extension is accomplished through the judicious selection of individual molecular building blocks for the donor, the acceptor, and the π -bridge.

One approach to optimizing the intramolecular charge transfer (ICT) process in $D-\pi-A$ sensitizer dye molecules has been to incorporate proaromatic structures. Here, we describe proaromaticity as the generation of a locally aromatic

Received: September 29, 2022 Revised: December 13, 2022 Published: December 28, 2022





Figure 1. Dyes studied with ground-state aromatic π -bridges having blue ring colors and excited-state aromatic π -bridges having green color. The anticipated relative kinetics based on aromaticity considerations are listed below the arrows.

motif after photoexcitation and subsequent charge separation, as shown in Figure 1. Proaromatic functionality provides additional stability and a lower photoexcitation energy through localized aromaticity in the excited state. This approach results in narrower optical band gaps, thus allowing for capture of NIR light. We previously introduced a sensitizing dye (PB1) using 3,4-thienothiophene $(3,4-TT)^{23-25}$ as a proaromatic-conjugated π -bridge. Devices incorporating PB1 demonstrated PCEs of up to 7.8% and longer wavelength absorption onset in solution at ~665 nm (compared to 5.9% PCE and a ~590 nm onset for the non-proaromatic analogues C1 and C213).^{26,27} Proaromaticity has also been implemented in DSC dye studies utilizing thienopyrazine (TPz)-28-31 and indolizine-^{22,32,33} based building blocks both experimentally and computationally. In general, dyes incorporating 3,4-TT-24,34,35 and TPz-36-40 based building blocks have shown exceptional promise in a variety of DSC devices. However, to the best of our knowledge, the effects of proaromaticity on excited-state kinetics have not been systematically probed. To better understand the influence of proaromaticity on the performance of sensitizer dyes in general and to facilitate the design of more efficient future molecular architectures, here we selectively probe the contributions of proaromaticity on the excited-state dynamics of a series of four ICT sensitizer dyes. Among the four dyes (shown in Figure 1), C213 utilizes a thiophene-based π -bridge that is not proaromatic, while PB1, NL6, and JW1 incorporate proaromatic π -bridging units.

In the studies presented here, C213 serves as a control due to the non-aromaticity of the traditional thiophene bridge in the excited state. The remaining dyes (PB1, NL6, and JW1) are expected to possess proaromatic π -bridging units, with the 3,4-TT moiety in PB1 exhibiting localized aromaticity in one of the thiophene rings after CT. In both NL6 and JW1, TPz is predicted to have localized aromaticity on the pyrazine ring after CT, as shown in Figure 1. The optical band gap is narrower in the proaromatic dyes than in C213, with the excitation energy having the following order from highest to lowest energy: C213 > PB1 > NL6/JW1. NL6 and JW1 have very similar optical energy gaps due to the similarity in their structures, but JW1 incorporates three triarylamine (TAA) donor groups compared to just one in NL6. The additional donor groups result in added higher energy transitions for a panchromatic absorption profile and could delocalize the cation after electron injection.³⁰ Two **NL6** derivatives are also synthesized and investigated where the cyanoacrylic acid moiety is replaced with either a dicyano (JW2) or diester

Scheme 1. Synthetic Route to JW2 and JW3

$$C_{6}H_{13}O$$

(JW3) group as the acceptor in order to rule out exciplex formation via hydrogen bonding (Scheme 1). Here, we use a combination of ultrafast transient absorption spectroscopy (TAS) and computational chemistry to connect the dye structure to excited-state dynamics in order to reveal the effects of proaromaticity on the lifetime.

MATERIALS AND CHARACTERIZATION

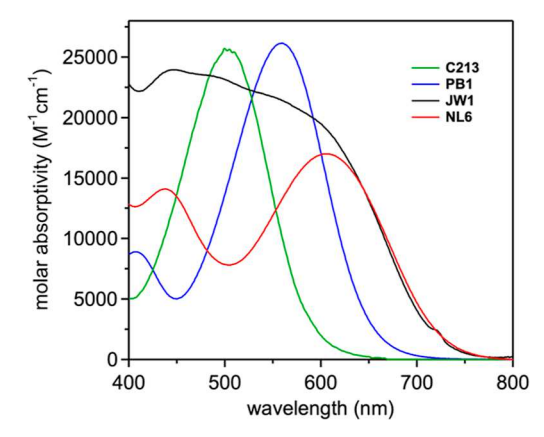
General Information. All commercially obtained reagents were used as received. Thin-layer chromatography (TLC) was conducted with Sorbtech silica XHL TLC plates and visualized with UV light. Column chromatography was performed using Sorbent Tech P60, 40–63 μ m (230 × 400 mesh). ¹H NMR spectra were recorded on Bruker Avance-300 (300 MHz) and Bruker Avance-400 (400 MHz) spectrometers. Data were reported as s = singlet, d = doublet, t = triplet, q = quartet, p = pentet, m = multiplet, br = broad, ap = apparent, and dd = doublet of doublets; coupling constant(s) in Hz; integration. Absorbance spectra were measured with a Cary 5000 UVvis-NIR spectrophotometer with a chloroform solution. FT-IR measurements were taken using a Bruker Alpha FT-IR spectrometer with an ATR attachment. For high resolution electrospray ionization (ESI) mass spectrometry, a TOF analyzer was used to collect the data in positive mode with the Waters Synapt HDMS instrument. Emission spectra were acquired using a Horiba QuantaMaster 8075-21. Light from a xenon lamp is monochromated in a dual diffraction grating setup before irradiating the sample in a glass cuvette. Emission is detected at a right angle from the excitation source by focusing the emitted light into a scanning diffraction grating and onto a photomultiplier tube. Spectroelectrochemistry data were collected with a honeycomb spectroelectrochemical cell system (Pine Research Instrumentation) using a 1 cm × 1 cm quartz cuvette (Pine Research part RRPG094), a Pt honeycomb electrode card (Pine Research part AB01STC1PT), an Ag/AgCl reference electrode (Pine Research part RRPEAGCL2), and a honeycomb cell cap (Pine Research part AC01STCCAP3). A mini-USB-to-Banana generic cable (Pine Research part RRPECBL2) connected the honeycomb

card to a potentiostat (CH Instruments Electrochemical Analyzer CHI600E). The light source (UV/Vis/NIR Light Source, Pine Research part RRAVSP) and spectrometer (AvaSpec-ULS2048-USB2-50 Spectrometer; Pine Research part RRAVSP3) were used in conjunction to the AvaSoft8 software program.

C213,²⁷PB1,⁴¹NL6,²⁸ and JW1³⁰ were prepared as previously described. JW2 and JW3 were prepared via Knoevenagel condensation as described below from aldehyde (1), which is a common intermediate in the NL6 synthesis (Scheme 1).²⁸

2-(4-(7-(4-(Bis(4-(hexyloxy)phenyl)amino)phenyl)-2,3-diphenylthieno[3,4-b]pyrazin-5-yl)benzylidene)malononitrile (JW2). Aldehyde 4-(7-(4-(bis(4-(hexyloxy)phenyl)amino)phenyl)-2,3-diphenylthieno[3,4-b]pyrazin-5yl)benzaldehyde $(1)^{28}$ (52 mg, 62.0 μ mol), malononitrile (5 mg, 68.0 μ mol), and 4-aminophenol (17 mg, 0.16 mmol) were dissolved in toluene (1.3 mL, 0.05 M) and acetic acid (10 μ L, 7.0 M). The reaction was refluxed using a Dean-Stark apparatus under N2 while stirring for 24 h. The product was isolated by extraction with a 1:1 dichloromethane/water mixture (40 mL) and the organics were rinsed three times. The organic layer was then dried over Na₂SO₄ and the solvent was removed by a rotary evaporator to give the crude material. The crude mixture was filtered through a pad of silica gel with a 65% dichloromethane/35% hexane mixture as the eluent for purification. JW2 was isolated as a blue solid (32 mg, 58% yield). 1 H NMR (400 MHz, DMSO): δ 8.52 (d, J = 8.6 Hz, 2H), 8.47 (s, 1H), 8.14 (d, J = 9.0 Hz, 2H), 8.07 (d, J = 8.8Hz, 2H), 7.54 (d, J = 6.0 Hz, 2 H), 7.49 (d, J = 6.4 Hz, 2H), 7.44-7.35 (m, 6H), 7.12 (d, J = 8.9 Hz, 4H), 6.96 (d, J = 9.0Hz, 4H), 6.85 (d, J = 8.9 Hz, 2H), 3.98 (t, J = 6.5 Hz, 4H), 1.74-1.70 (m, 4H), 1.43-1.20 (m, 12H), 0.91-0.86 (ap m, 6H) ppm. IR (neat, cm⁻¹): 2953, 2919, 2853, 1709, 1599, 1565, 1502, 1352, 1232 cm⁻¹. HRMS ESI (positive mode) m/z: calcd for C₅₈H₅₃N₅O₂S [M]⁺, 883.3926; found, 883.3920.

Diethyl 2-(4-(7-(4-(Bis(4-(hexyloxy)phenyl)amino)-phenyl)-2,3-diphenylthieno[3,4-b]pyrazin-5-yl)-benzylidene)malonate (JW3). Starting aldehyde 4-(7-(4-



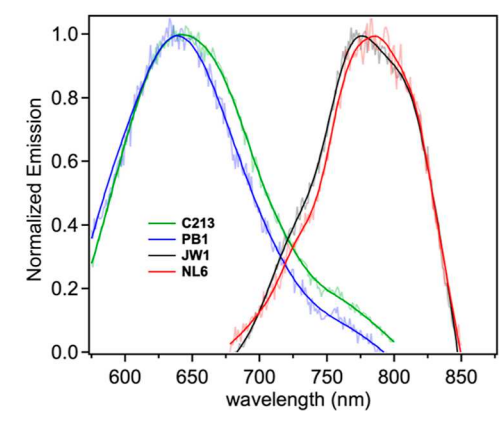


Figure 2. Absorption spectra (left) and emission spectra (right) for C213, PB1, NL6, and JW1. The emission data are plotted with both non-fitted data (light color) and fitted with an LOESS function (2nd order 0.3 smoothing factor) as the darker color. The abrupt fall off of the emission curves for NL6 and JW1 is due to the spectral limit of the photomultiplier tube in the fluorimeter. Spectra are collected in chloroform at room temperature. Emission spectra are collected at a concentration of 1.1×10^{-5} M.

(bis(4-(hexyloxy)phenyl)amino)phenyl)-2,3-diphenylthieno-[3,4-b]pyrazin-5-yl)benzaldehyde $(1)^{28}$ (108 mg, 0.13 mmol) and diethyl malonate (67 mg, 0.39 mmol) were dissolved in CHCl₃ (2.6 mL, 0.05 M) and piperidine (77 mg, 0.91 mmol) under N2. The reaction was heated to 80 °C in a sealed vial and stirred for 18 h. The product was extracted with a 1:1 dichloromethane/water mixture (40 mL) and the organics were rinsed three times and the organic layer was dried over Na₂SO₄. After the removal of solvent under reduced pressure, the crude mixture was subjected to silica gel flash chromatography for purification with a 70% dichloromethane/30% hexane mixture as the eluent. JW3 was isolated as a green solid (44 mg, 35% yield). ¹H NMR (300 MHz, DMSO): δ 8.37 (d, J = 8.8 Hz, 2H), 8.13 (d, J = 9.0 Hz, 2H), 7.74 (s, 1H), 7.65 (d, I = 8.4 Hz, 2H), 7.52–7.35 (m, 10 H), $7.12 \text{ (d, } J = 9.0 \text{ Hz, } 4\text{H}), 6.96 \text{ (d, } J = 9.1 \text{ Hz, } 4\text{H}), 6.86 \text{ (d, } J = 9.1 \text{ Hz, } 4\text{Hz, } 4\text{H}), 6.86 \text{ (d, } J = 9.1 \text{ Hz, } 4\text{Hz, } 4\text{$ 8.9 Hz, 2H), 4.38 (q, J = 7.1 Hz, 2H), 4.30 (q, J = 7.1 Hz, 2H), 3.98 (t, J = 6.3 Hz, 4H), 1.74-1.68 (m, 4H), 1.43-1.24 (m, 18H), 0.91-0.86 (ap m, 6H) ppm. IR (neat, cm⁻¹): 2953, 2919, 2853, 1709, 1599, 1565, 1502, 1352, 1232 cm⁻¹. HRMS ESI (positive mode) m/z: calcd for $C_{62}H_{63}N_3O_6S$ [M + H]⁺, 978.4516; found, 978.4530.

Transient Absorption Spectroscopy. Femtosecond transient absorption spectra and kinetics were acquired using a Helios fsTAS spectrometer from Ultrafast Systems. In order to generate the excitation pulses for each of the four samples, the 800 nm (<100 fs FWHM) fundamental output from a femtosecond amplifier (Coherent Astrella) was routed into an optical parametric oscillator (Light Conversion Topas). The actinic beam wavelength was selected based on the groundstate absorption of each dye in the series. By irradiating the solutions and films with photons of energy matching the maximum absorbance (λ_{\max}^{abs}) of each dye S_0 to S_1 state transition energy, a high concentration of transient species is generated allowing for a maximum possible signal to be detected. Probe beams were generated by taking a portion of the 800 nm fundamental and focusing them into CaF2 and YAG crystals for the visible and NIR regions, respectively. By generating the probe in this manner, the temporal characteristics of the fundamental beam are preserved in the broadband continua. Pump and probe beams are spatially overlapped in the sample, while the time delay between the actinic and probe beams is controlled by a mechanical optical delay line (0.02 ps

step size). Solutions were prepared at an approximate concentration of 0.1 mM under an ambient atmosphere.

TAS film studies were conducted with sealed electrodes similarly to previously described.⁴² The sensitizing solutions were JW1 (0.3 mM dye, 3 mM CDCA, 7:3 EtOH/CHCl₃), PB1 (0.3 mM dye, 12 mM CDCA, 4:1 EtOH/THF), C213 (0.2 mM dye, 8 mM CDCA, 4:1 EtOH/THF), and NL6 (0.2 mM dye, 4:1 EtOH/THF) where each dye was sensitized for 18 h before use. The inert electrolyte used was composed of 1.0 M 1-butyl-3-methylimidazolium tetrafluoroborate, 0.5 M 4tert-butylpyridine (TBP), 0.1 M guanidinium thiocyanide (GuNCS), and 1.0 M lithium bis(trifluoromethanesulfonyl)imide (LiTFSI) in acetonitrile:valeonitrile (85:15, v/v) solvent. TAS data of the dyes adsorbed to the TiO₂ surface under an inert electrolyte were obtained in a very similar manner, but due to the extended lifetime of the signal, the probe was generated in a white fiber laser and the delay between the pump and probe beams was controlled electronically. This allows for measurements with similar IRF compared to the method described previously while extending measurements beyond the approximately 8 ns delay range afforded by the physical length of the mechanical delay stage. To ensure that no photobleaching occurred during acquisition, each individual scan within an averaged spectrum was analyzed for any decrease in signal intensity or change in wavelength or temporal values (Figure S16).

Single wavelength kinetics were fit with the Kohlrausch-Williams-Watts (KWW) function

$$\Delta OD(t) = \Delta OD_{t=0} e^{-\left(\frac{t}{\tau_{KWW}}\right)^{\beta}}$$
(1)

where $\Delta \mathrm{OD}_{t=0}$ represents the change in optical density at time zero, au_{KWW} is the stretched exponential lifetime, and eta is the stretch parameter, range in value from 0 to 1.^{43–46} The observed lifetime is calculated from the fitting parameters using a gamma function distribution of eta^{-1} (eqs 2 and 3).

$$\Gamma(x) = \int_0^\infty u^{(x-1)} e^{-x} du$$
 (2)

$$\tau_{\rm obs} = \frac{\tau}{\beta} \Gamma \left(\frac{1}{\beta} \right) \tag{3}$$

The use of a KWW fitting approach is commonly used in the dye-sensitized surface literature; it assumes a Levy distribution

of kinetics, adequately compensating for the multiple complex, weighted processes competing within a DSC device. 47,48

Computational Methodology. The B3LYP^{49,50} hybrid density functional theory (DFT) method was used in conjunction with the 6-311+G(d_p) basis set⁵¹ to compute all DFT and time-dependent DFT (TD-DFT) data reported herein using the Gaussian16⁵² software package with default convergence criteria. The gauge-independent atomic orbital (GIAO) method was used to compute the B3LYP/6-311+G(d_p) magnetic shielding tensors. S3,54 Harmonic vibrational frequency computations were performed to verify each ground-state structure as a minimum on the B3LYP/6-311+G(d_p) potential energy surface.

RESULTS AND DISCUSSION

Steady-State Optical Properties. Absorbance spectra for C213, PB1, NL6, and JW1 are compared, as shown in Figures 2 and S1–S4. Metrics for these spectra are tabulated in Table 1. C213 shows the highest energy absorption onset (λ_{onset}^{abs})

Table 1. Summary of Steady-State Optical and Electrochemical Properties of C213, PB1, NL6, and JW1^a

dye	$\lambda_{\max}^{abs} \choose (nm)$	$\lambda_{ ext{onset}}^{ ext{abs}} $ $(ext{nm})$	$\lambda_{\max}^{em} \choose nm$	$\frac{E_{(0-0)}}{(eV)}$	$\varepsilon (\mathrm{M^{-1} cm^{-1}})$
C213	500	580	641	2.17	26,000
PB1	553	650	639	2.07	26,000
NL6	604	720	786	1.75	17,000
JW1	590 (sh)	720	776	1.76	21,000

[&]quot;Data are collected in chloroform. "sh" indicates shoulder. The $E_{(0-0)}$ values are found by taking a line of best fit along the low energy side of the absorption spectrum (Figures S1–S4).

of the series (580 nm; see Figure S1), which is expected from the general trend of proaromatic structures absorbing longer wavelength photons than non-proaromatic building blocks of a similar conjugation length. The proaromatic 3,4-TT unit in **PB1** induces a bathochromic shift in the absorption to an onset

of 650 nm. Finally, TPz further red-shifts the absorption onset in NL6 and JW1 to past 720 nm. The inclusion of two additional donor groups in JW1 also broadens its absorption spectrum with added high energy transitions compared to that of NL6 and provides a modest increase in molar absorptivity. The onsets of absorption are used for the comparisons mentioned above since the absorption maximum $(\lambda_{\text{max}}^{\text{abs}})$ for the lowest energy transition of JW1 presents as a poorly defined shoulder due to nearby higher energy transitions.

Emission spectra of all four dyes in chloroform are included in Figure 2. As expected from their absorption profiles, NL6 and JW1 peaks emit at lower energies (~780 nm) compared to both C213 and PB1 (\sim 640 nm). The emission profile of both JW1 and NL6 abruptly end near 850 nm due to the limitations in the quantum efficiency of the photomultiplier tube-based detector in this region of the spectrum. The $E_{(0-0)}$ values are taken as the intercept of the absorption spectrum and normalized emission spectrum (Figures S1-S4) range from 2.17 to 1.75 eV and follow the trend C213 > PB1 > JW1 \cong NL6 with a 0.1 eV difference in C213 and PB1 and a 0.32 eV difference between PB1 and NL6. The $E_{(0-0)}$ values of NL6 and JW1 are near identical. These $E_{(0-0)}$ values are used to assess the changes in optical energy gaps in relation to excitedstate lifetimes below. A complete energy diagram for the sensitizers and TiO₂ can be found in Figure S7.

Ultrafast Excited-State Dynamics. Femtosecond transient absorption spectroscopy (fsTAS) experiments were performed on the dyes in chloroform (Figures 3 and 4, Table 2) after initial spectroelectrochemical (SEC) measurements (Figures S1–S6). Solutions of acetonitrile/tetrahydrofuran (70%/30% by volume since the dyes were not fully soluble in pure acetonitrile) were also used to probe the effects of different dielectric environments on the dye excited states (Figures S10–S13, Table S1). Similar trends were observed in acetonitrile/tetrahydrofuran, and so, only the chloroform results are presented in the main text. Probe wavelengths for each sample were selected at or near the maximum of excited-state absorption. For JW1 in solution, this necessitated the use

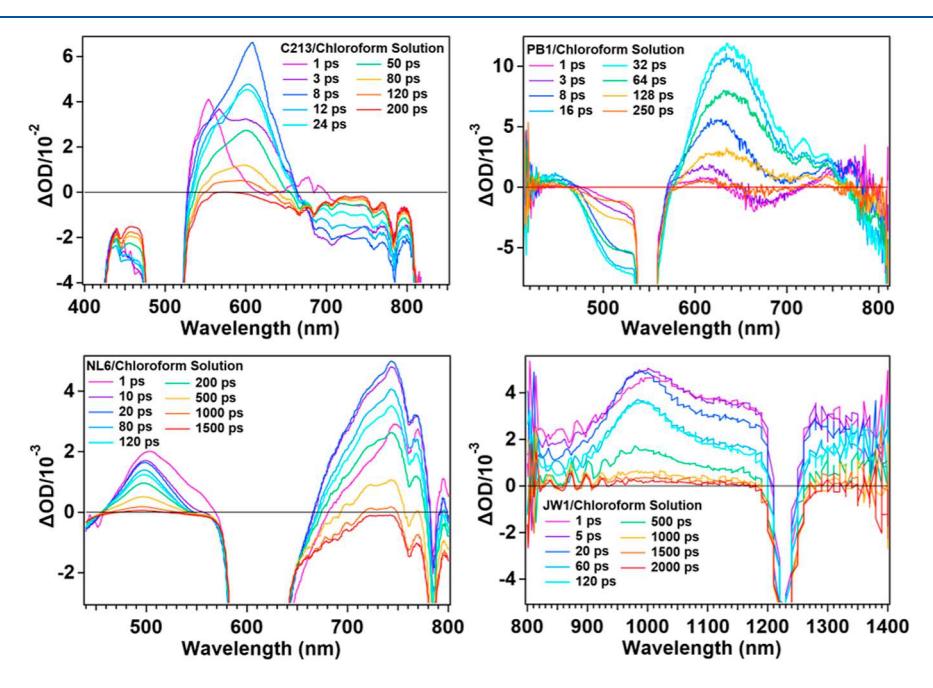


Figure 3. Femtosecond transient absorption spectra of C213, PB1, NL6, and JW1 in chloroform.

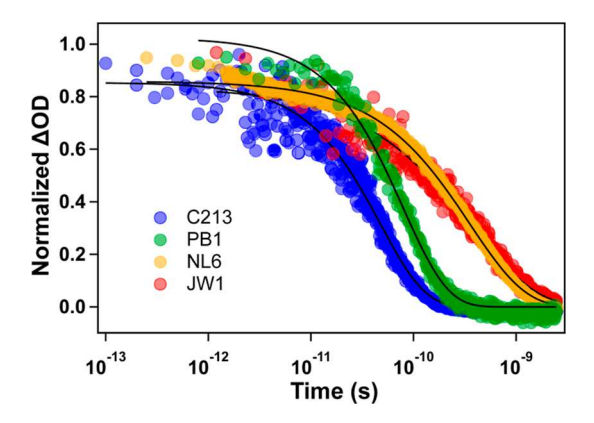


Figure 4. Femtosecond transient absorption kinetics of **C213**, **PB1**, **NL6**, and **JW1** in chloroform presented with the time axis in log scale. Lifetime constants were extracted from stretched exponential decay functions with an *x*-offset to only perform the regression on data from the maxima onward.

Table 2. fsTAS Solution Kinetics in Chloroform

dye	pump (nm)	probe (nm)	$ au_{ m obs}~(m ps)$
C213	505	610	47.5
PB1	550	610	81.4
NL6	605	735	338.8
JW1	610	999	456.5
JW2	610	725	234.6
JW3	610	745	720.8

of the NIR probe region as the induced absorption was very broad and extended beyond the limit of the visible probe. C213 and PB1 show similar strong transient absorption features near 650 nm with the ground-state bleach (GSB) of PB1 being more easily distinguished. In both cases, the transient absorption feature (and the GSB of PB1) returns to a near 0 ΔA value at longer time lengths indicating the return of the dye to the ground state. However, the excited-state lifetime of PB1 was approximately twice as long as C213 (81 ps vs 48 ps in CHCl₃). The transient absorption spectrum of NL6 shows a relatively strong feature near 740 nm, which has a decay rate of 339 ps. The excited-state lifetime of NL6 was found to be more than four times longer than that of PB1, which suggests that the TPz group promotes longer excitedstate lifetimes than the 3,4-TT building block. The transient absorption feature of JW1 that is the strongest in the spectrum is near 1000 nm, which clearly returns to 0 ΔA at long time scales. JW1 was found to have the longest excited-state lifetime of 457 ps, which is similar to that of NL6 at about 1.3× longer than the excited-state lifetime of NL6 at 339 ps. Contrary to what would be expected by the energy gap law, it was observed that the lower the energy gap in this series, the longer the observed lifetime in solution (JW1 > NL6 > PB1 > C213). Notably, the dyes incorporating presumably proaromatic groups (TPz and 3,4-TT) have the longest excited-state lifetimes despite absorbing lower energy light where excitedstate lifetimes would be predicted to be shorter. The following trends are observed according to π -bridge functionality (Figure

excited state lifetime trend: TPz > 3, 4-TT > thiophene optical energy gap trend: TPz < 3, 4-TT < thiophene

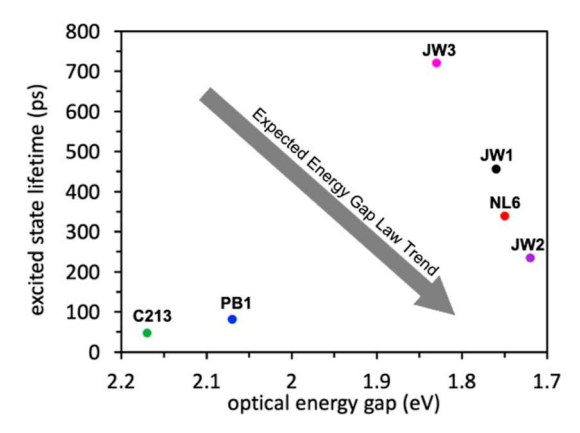


Figure 5. Comparison of the expected trend of excited-state lifetime vs optical energy gap via the energy gap law to the data points observed in this study.

(for spectra of JW2 and JW3; see Figures S8 and S9.) Irregularities in the shape of early time-delay spectra arise from coherent artifacts at or near time-zero. Negative dA values for C213 beyond 650 nm are attributed to noise and were not used for the kinetic analysis.

Given the observation of an unexpected trend relative to that predicted by the energy gap law, several control experiments were conducted to probe if the observed trend is due to molecular design, aggregation, or hydrogen bonding. Since the TPz building block has basic nitrogen functionality present not on the thiophene or 3,4-TT building block, hydrogen-bonding interactions are possible with the carboxylic acid group on JW1 or NL6. Thus, JW2 and JW3 were synthesized (Scheme 1) to remove the carboxylic acid group. JW2 uses two cyano acceptor groups, while JW3 uses two ester groups in place of the cyanoacetic acid group of NL6. These dyes both absorb near NL6 and JW1, with JW2 being notably shifted toward longer wavelengths (Figures S5 and S6). Both JW2 and JW3 have similar transient absorption spectra to NL6, which is expected from direct analogues (Figures S8 and S9, respectively). The lifetime of JW2 (235 ps) is roughly half that of NL6 (457 ps). However, $E_{(0-0)}$ is appreciably lower than that of C213 and an excited-state lifetime 4.9× longer is observed with JW2. JW3 has the longest lifetime of the dyes examined at 721 ps or 15.2× longer than C213. Thus, potential hydrogen bonding from the carboxylic acid of NL6 or JW1 cannot be the reason for the longer lifetimes observed relative to C213 and PB1 since analogues of NL6 with no carboxylic acid group show comparable or longer lifetimes.

Emission spectra of NL6 and JW1 at two different concentrations were also collected in chloroform (Figure S17) to determine if the observed optical properties of these two dyes are influenced by the formation of aggregates in the excited state. Aggregates are well known to extend excited-state lifetimes and their formation is likely to cause noticeable changes in the emission profile. At both high $(1.1 \times 10^{-5} \text{ M})$ and low $(1.1 \times 10^{-7} \text{ M})$ concentrations, both dyes showed minimal changes in their emission. As such, the enhanced excited-state lifetimes of JW1 and NL6 are attributed to a molecular design principle rather than some type of intermolecular interaction since no concentration effects on spectra shape were observed.

Excited-state aromaticity has been previously examined for dye PB1 via nucleus independent chemical shift (NICS) analysis, with results revealing appreciable aromaticity in the

Table 3. Bond-Length Analysis of the TPz Bridge in NL6 and JW1 in the Ground-State Singlet (S_0) , the First Excited Singlet (S_1) , and the First Excited Triplet State (T_1)

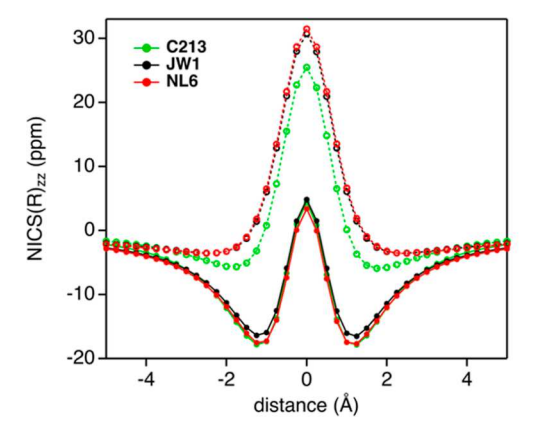
bond ^a	S_0 (Å)	S ₁ (Å)	$\Delta R_{\rm S1} ({\rm \AA})$	T_1 (Å)	$\Delta R_{\mathrm{T1}} \; (\mathrm{\AA})$	valence bond theory prediction (calculated
				NL6		
R(2,3)	1.4062	1.4007	-0.0055	1.4494	0.0432	lengthens (T1 agrees)*
R(3,8)	1.4392	1.4467	0.0075	1.4225	-0.0167	shortens $(T_1 \text{ agrees})^*$
R(3,4)	1.3561	1.3550	-0.0011	1.3222	-0.0339	shortens (S_1 and T_1 agree)
R(4,5)	1.3147	1.3359	0.0212	1.3784	0.0637	lengthens $(S_1 \text{ and } T_1 \text{ agree})$
R(5,6)	1.4613	1.4271	-0.0342	1.3845	-0.0768	shortens $(S_1 \text{ and } T_1 \text{ agree})$
R(6,7)	1.3146	1.3398	0.0252	1.3888	0.0742	lengthens $(S_1 \text{ and } T_1 \text{ agree})$
R(7,8)	1.3591	1.3406	-0.0185	1.3016	-0.0575	shortens $(S_1 \text{ and } T_1 \text{ agree})$
R(8,9)	1.4023	1.4206	0.0183	1.4942	0.0919	lengthens $(S_1 \text{ and } T_1 \text{ agree})$
				JW1		
R(2,3)	1.4048	1.4020	-0.0028	1.4407	0.0359	lengthens (T1 agrees)*
R(3,8)	1.4385	1.4539	0.0154	1.4265	-0.0120	shortens $(T_1 \text{ agrees})$
R(3,4)	1.3573	1.3560	-0.0013	1.3300	-0.0273	shortens $(S_1 \& T_1 \text{ agree})$
R(4,5)	1.3157	1.3310	0.0153	1.3617	0.0460	lengthens $(S_1 \text{ and } T_1 \text{ agree})$
R(5,6)	1.4665	1.4182	-0.0483	1.4083	-0.0582	shortens $(S_1 \text{ and } T_1 \text{ agree})$
R(6,7)	1.3169	1.3409	0.0240	1.3632	0.0463	lengthens $(S_1 \text{ and } T_1 \text{ agree})$
R(7,8)	1.3584	1.3407	-0.0177	1.3200	-0.0384	shortens (S ₁ and T ₁ agree)
R(8,9)	1.4032	1.4184	0.0152	1.4608	0.0576	lengthens $(S_1 \text{ and } T_1 \text{ agree})$

²See Figure 6 for bond numbering scheme. *S₁ calculation suggests minimal change.

Figure 6. Valence bond theory suggested bond length changes upon intramolecular charge transfer if aromaticity increases in the excited state.

excited state for the green colored ring in Figure 1.41 This observation suggests that proaromatic functionality could be a contributing factor toward the longer excited-state lifetime of PB1 relative to C213 as discussed above. To probe this correlation further, a similar NICS analysis was undertaken with NL6 and JW1 to probe the aromaticity in the singlet ground state (S_0) , the first excited singlet state (S_1) , and the first excited triplet state (T_1) of the TPz-based dyes. Valence bond theory suggests that the pyrazine ring in the TPz building block of NL6 and JW1 will exhibit excited-state aromatic behavior after photoinduced ICT, as shown in Figure 1. Upon a photoinduced ICT event, the bond lengths on the TPz π bridge would be expected to change, as listed in Table 3 and Figure 6. The double bonds of the ground-state thiophene ring (2,3 and 8,9) would be expected to shift toward longer bond lengths, while the single bond (3,8) would be expected to shorten in the excited state upon charge transfer. The pyrazine ring would be expected to generate an aromatic structure in the excited state with reduced bond length alternations relative to the ground state causing the double bonds (4,5 and 6,7) to lengthen and the single bonds to shorten (3,4; 5,6; and 7,8).

Comparing the S_0 to the T_1 geometry, all of these predictions via valence bond theory agree with those observed via DFT. A similar observation is made about the S₀ and S₁ geometries with notable exceptions at the 2,3 and 3,8 bonds. Notably, minimal change is expected (0.0068 Å or about an order of magnitude less than the larger changes observed) for these bonds via DFT. Additionally, in the excited state of the TPzbased dyes, the bond lengths in the thiophene ring deviate away from uniformity, while those of the pyrazine become more homogenous as observed by bond length alternation (BLA) values (see Tables S2-S6 for full summary and sample calculations). For the thiophene ring of C213, NL6, and JW1, the BLA value is 0.1507-0.1517 Å in the S₀ state and increases for the S_1 (0.1518–0.1583 Å) and T_1 (0.1519–0.1690 Å) states, indicating that the structures have reduced aromaticity with more alternation of bond lengths as anticipated by valence bond theory. Importantly, the pyrazine ring of NL6 and JW1 shows the opposite trend with less BLA in the S_1 (0.0660– 0.0668 Å) and T_1 (0.0616–0.0625 Å) states than the S_0 (0.0904-0.0908 Å) state, indicating that the pyrazine ring shows an increase in aromaticity in the excited state. These



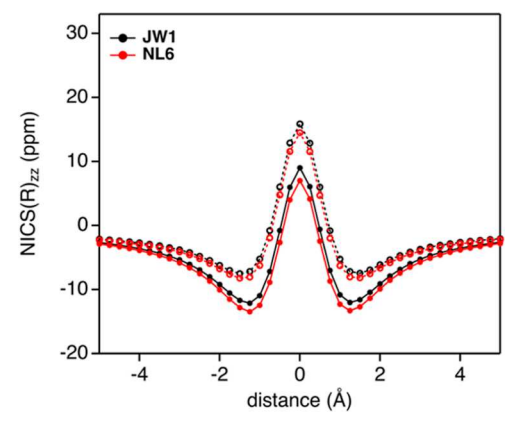


Figure 7. NICS(R)_{zz} vs distance from the center of the thiophene ring (left) of C213, NL6, and JW1 and the pyrazine ring (right) of NL6 and JW1. The S_0 -state calculations are shown as solid lines with closed markers. The T_1 -state calculations are shown as dashed lines with open markers. Note: the S_0 -state thiophene ring NICS calculation for C213 and NL6 nearly completely overlap.

results indicate that the thiophene ring loses its aromaticity from the ground state after ICT occurs, but that the pyrazine maintains aromatic nature and thus provides stability to the excited-state species by gaining aromaticity.

As an additional means to probe the excited-state aromaticity, NICS(R)zz values were computed for the two rings of the TPz group without substitution, within the NL6 and JW1 dyes, and for the thiophene in C213 (Figures 7, S18 and S19). The T1 state is used in these calculations as previously described because the computation of NMR shielding tensors is not currently available in Gaussian 16 for the TD-DFT methods used in this study to directly assess the S1 state. 41 The chemical shifts are computed from 5 Å above the plane of the ring being examined to 5 Å below the plane of the ring in 0.25 Å increments. As is typically observed with aromatic structures via NICS(R)zz calculations, the chemical shift becomes increasingly negative as the center of the ring is approached until about ± 1 Å above or below the plane of the ring as is observed for the ground-state $NICS(R)_{77}$ calculations represented as full lines in Figure 7. In all cases, unsubstituted TPz, NL6-TPz, JW1-TPz, and thiophene of C213, the thiophene rings, and pyrazine rings (when present) show aromaticity via NICS analysis in the S₀ state. Analysis of the T₁ state (dashed lines in Figure 7), no aromaticity is observed for either the thiophene or pyrazine ring of TPz. Indeed, significantly antiaromatic (+ppm) values near 30 ppm at ±1 Å from the center of the thiophene ring plane are observed, which agrees with Baird's rule, which predicts that aromatic structures become antiaromatic in the excited state (Figures S18 and S19). 56-60 For the C213 dye, the thiophene ring is observed to lose aromaticity in the T1 state, showing approximately 0 ppm at ± 1 Å from the center of the thiophene ring plane. The same observations are made with respect to the thiophene rings of the TPz groups in NL6 and JW1. However, the pyrazine ring on the TPz groups of NL6 and JW1 shows retained aromaticity in the T1 state, which is consistent with the proaromatic behavior suggested by valence bond theory. Thus, the three dyes with groups, which show appreciable proaromatic behavior via bond length and NICS analyses (PB1, NL6, and JW1), all have substantially longer excited-state lifetimes than the dye without proaromatic groups (C213). This proaromatic property is correlated to both longer excited-state lifetimes and longer wavelength absorption in solution, both of which are important to many dyesensitized applications.

Surface Studies. To probe the effects of proaromaticity on interfacial charge separation durations, nanosecond TAS experiments were undertaken by anchoring C213, PB1, NL6, and JW1 to a TiO2 surface. Upon photoexcitation of a dye anchored to TiO₂ (eq 4), an electron can be injected into the TiO₂ conduction band (eq 5). In the presence of an inert electrolyte (no redox shuttle present), the back electron transfer reaction from reduced TiO2 to the anchored dye cation can be monitored via decay of the dye cation signal (eq 6). By monitoring the rate of back electron transfer, the effects of proaromaticity can be indirectly probed on the cationic state. Aromaticity could be expected to extend charge separation duration across an interface by stabilizing the cationic state at the surface similar to that observed via ICT events where aromaticity stabilizes cationic and anionic localized states.

$$Dye-TiO_2 + h\nu \rightarrow Dye^*-TiO_2 \text{ (excitation)}$$
 (4)

$$Dye^*-TiO_2 \rightarrow Dye^+-TiO_2(e^-) \text{ (injection)}$$
 (5)

$$Dye^+-TiO_2(e^-) \rightarrow Dye-TiO_2$$
 (back electron transfer) (6

Table 4 summarizes the interfacial kinetics observed via nsTAS (Figure S15). A back electron transfer reaction rate for

Table 4. nsTAS Surface Kinetics

dye	pump (nm)	probe (nm)	$ au_{ m obs} \; (\mu m s)$
C213	505	765	31.9
PB1	550	700	257.9
NL6	605	830	40.2
JW1	610	780	152.7

C213 is observed at 31.9 μ s. Interestingly, all of the proaromatic structure containing dyes lead to extended photoinduced interfacial charge separation lifetimes (PB1: 257.9 μ s, NL6: 40.2 μ s, JW1: 152.7 μ s). Among the proaromatic structure containing dyes, 3,4-TT-derived PB1 has an appreciably longer charge separated state lifetime than the TPz-based dyes JW1 and NL6. The large difference in excited-state lifetimes between JW1 and NL6 suggests that JW1 may be able to delocalize its excited-state cation across the three triarylamine groups, compared to just one in NL6 to extend the interfacial charge separated lifetime since the

remaining components of the structures are identical. This could provide additional stabilization of the cationic excited state and prevent the approximately 4× more rapid back electron transfer reaction observed in NL6. Interestingly, the trend in excited-state lifetimes observed in solution (JW1 > NL6 > PB1 > C213) is not observed on the film interface. We stress that this is only an initial probing of the effects of proaromaticity at a surface and that a number of factors also contribute to the rate of back electron transfer including dye orientation, dye-dye packing distances that can allow for hole migration, and distance of the oxidized region of the dye from the TiO2 surface. However, overall, these surface studies provide an initial probe into the influence proaromaticity may have on charge separation durations at semiconductor surfaces in addition to the extended excited-state lifetimes observed in solution with ICT-based dyes.

CONCLUSIONS

A series of dye analogues were studied with a non-proaromatic thiophene π -bridge, a proaromatic thieno [3,4-b] thiophene π bridge, and a proaromatic thieno [3,4-b] pyrazine π -bridge. The dyes with a proaromatic π -bridge were found to have lower excitation energies from the S_0 to S_1 states in solution, while dramatically increasing the excited-state lifetimes of the dyes as observed via femtosecond transient absorption spectroscopy. This is contradictory to the expected trend based on the energy gap law, which indicates that the molecular structure of these compounds plays a larger role in controlling dye excitedstate lifetimes than the energy gap between the S_0 and S_1 states. The increased excited-state lifetime is correlated to the inclusion of proaromatic groups, and computational results confirm the proaromatic nature of the series of dyes studied here both by an analysis of their bond length and NICS(R)₇₂ calculations. At a TiO₂ interface, the dyes with proaromatic groups were observed to have prolonged photoinduced charge separated states via nanosecond and femtosecond transient absorption spectroscopies. This study provides early indicators that proaromaticity may have significant effects on excited-state lifetimes for intramolecular charge transfer dyes and may prolong interfacial charge separation events. Future studies are aimed at probing additional proaromatic structures and attempting to quantify a correlation of aromaticity stabilization energy to lifetime by identifying a suitable pool of dyes with similar excitation energies to disentangle the effects of proaromaticity from the energy gap law with respect to excited-state lifetimes.

ASSOCIATED CONTENT

3 Supporting Information

The Supporting Information is available free of charge at https://pubs.acs.org/doi/10.1021/acs.jpcc.2c06906.

Steady-state optical properties, spectroelectrochemical studies, femtosecond transient absorption spectroscopy data (solution and surface), bond length analyses, NICS (R) $_{zz}$ analysis, NMR spectra, and TD-DFT data (PDF)

AUTHOR INFORMATION

Corresponding Authors

Gregory S. Tschumper — Department of Chemistry and Biochemistry, University of Mississippi, University, Mississippi 38677, United States; orcid.org/0000-0002-3933-2200; Email: tschumpr@olemiss.edu

Jared H. Delcamp — Department of Chemistry and Biochemistry, University of Mississippi, University, Mississippi 38677, United States; Orcid.org/0000-0001-5313-4078; Email: delcamp@olemiss.edu

Nathan I. Hammer — Department of Chemistry and Biochemistry, University of Mississippi, University, Mississippi 38677, United States; Orcid.org/0000-0002-6221-2709; Email: nhammer@olemiss.edu

Authors

Austin L. Dorris – Department of Chemistry and Biochemistry, University of Mississippi, University, Mississippi 38677, United States

Jonathon Watson — Department of Chemistry and Biochemistry, University of Mississippi, University, Mississippi 38677, United States; orcid.org/0000-0003-4307-0730

Jacquelyn J. Mosely — Department of Chemistry and Biochemistry, University of Mississippi, University, Mississippi 38677, United States

Ethan C. Lambert – Department of Chemistry and Biochemistry, University of Mississippi, University, Mississippi 38677, United States

Complete contact information is available at: https://pubs.acs.org/10.1021/acs.jpcc.2c06906

Author Contributions

A.L.D. and J.W. contributed equally. The manuscript was written through contributions of all authors. All authors have given approval to the final version of the manuscript. The authors declare that they have no known competing financial interests or personal relationships that could have appeared to influence the work reported in this paper.

Funding

This letter has been supported by the National Science Foundation (OIA-1757220, CHE-1954922, NSF AGEP 2111582, and CHE-2154403).

Notes

The authors declare no competing financial interest.

ACKNOWLEDGMENTS

The authors want to thank the National Science Foundation grant Numbers OIA-1757220, CHE-1954922, NSF AGEP 2111582, and CHE-2154403 for financial support.

REFERENCES

- (1) Chen, Y.; Zheng, Y.; Jiang, Y.; Fan, H.; Zhu, X. Carbon-Bridged 1,2-Bis(2-thienyl)ethylene: An Extremely Electron Rich Dithiophene Building Block Enabling Electron Acceptors with Absorption above 1000 nm for Highly Sensitive NIR Photodetectors. *J. Am. Chem. Soc.* 2021, 143, 4281–4289.
- (2) Ren, H.; Chen, J. D.; Li, Y. Q.; Tang, J. X. Recent Progress in Organic Photodetectors and their Applications. *Adv. Sci.* **2020**, *8*, 2002418.
- (3) Yao, Y.; Chen, Y.; Wang, H.; Samori, P. Organic photodetectors based on supramolecular nanostructures. *SmartMat* **2020**, *1*, No. e1009.
- (4) Yu, Z.; Li, F.; Sun, L. Recent advances in dye-sensitized photoelectrochemical cells for solar hydrogen production based on molecular components. *Energy Environ. Sci.* **2015**, *8*, 760–775.
- (5) Luciani, G.; Imparato, C.; Vitiello, G. Photosensitive Hybrid Nanostructured Materials: The Big Challenges for Sunlight Capture. *Catalysts* **2020**, *10*, 103.

- (6) Liu, X.; Inagaki, S.; Gong, J. Heterogeneous Molecular Systems for Photocatalytic CO2 Reduction with Water Oxidation. *Angew. Chem., Int. Ed.* **2016**, *55*, 14924–14950.
- (7) Li, S.; Zhang, H.; Yue, S.; Yu, X.; Zhou, H. Recent advances in non-fullerene organic photovoltaics enabled by green solvent processing. *Nanotechnology* **2021**, *33*, 072002.
- (8) Wang, X.; Sun, Q.; Gao, J.; Wang, J.; Xu, C.; Ma, X.; Zhang, F. Recent Progress of Organic Photovoltaics with Efficiency over 17%. *Energies* **2021**, *14*, 4200.
- (9) Biaggio, I. The Appeal of Small Molecules for Practical Nonlinear Optics. *Chem.—Eur. J.* **2022**, 28, No. e202103168.
- (10) Friedman, H. C.; Cosco, E. D.; Atallah, T. L.; Jia, S.; Sletten, E. M.; Caram, J. R. Establishing design principles for emissive organic SWIR chromophores from energy gap laws. *Chem* **2021**, *7*, 3359–3376.
- (11) Muñoz-García, A. B.; Benesperi, I.; Boschloo, G.; Concepcion, J. J.; Delcamp, J. H.; Gibson, E. A.; Meyer, G. J.; Pavone, M.; Pettersson, H.; Hagfeldt, A.; et al. Dye-sensitized solar cells strike back. *Chem. Soc. Rev.* **2021**, *50*, 12450–12550.
- (12) Siebrand, W. Radiationless Transitions in Polyatomic Molecules. I. Calculation of Franck-Condon Factors. *J. Chem. Phys.* **1967**, *46*, 440–447.
- (13) Siebrand, W. Radiationless Transitions in Polyatomic Molecules. II. Triplet-Ground-State Transitions in Aromatic Hydrocarbons. *J. Chem. Phys.* **1967**, *47*, 2411–2422.
- (14) Englman, R.; Jortner, J. The Energy Gap Law for Radiationless Transitions in Large Molecules. *Mol. Phys.* **1970**, *18*, 145–164.
- (15) Caspar, J. V.; Sullivan, B. P.; Kober, E. M.; Meyer, T. J. Application of the energy gap law to the decay of charge transfer excited states, solvent effects. *Chem. Phys. Lett.* **1982**, *91*, 91–95.
- (16) Caspar, J. V.; Meyer, T. J. Application of the Energy Gap Law to Nonradiative, Excited-State Decay. *J. Phys. Chem.* **1983**, *87*, 952–957.
- (17) Brogdon, P.; Cheema, H.; Delcamp, J. H. Near-Infrared-Absorbing Metal-Free Organic, Porphyrin, and Phthalocyanine Sensitizers for Panchromatic Dye-Sensitized Solar Cells. *ChemSusChem* **2018**, *11*, 86–103.
- (18) Suryani, O.; Higashino, Y.; Sato, H.; Kubo, Y. Visible-to-Near-Infrared Light-Driven Photocatalytic Hydrogen Production Using Dibenzo-BODIPY and Phenothiazine Conjugate as Organic Photosensitizer. ACS Appl. Energy Mater. 2018, 2, 448–458.
- (19) Ho, P. Y.; Mark, M. F.; Wang, Y.; Yiu, S. C.; Yu, W. H.; Ho, C. L.; McCamant, D. W.; Eisenberg, R.; Huang, S. Panchromatic Sensitization with Zn II Porphyrin-Based Photosensitizers for Light-Driven Hydrogen Production. *ChemSusChem* **2018**, *11*, 2517–2528.
- (20) Hardin, B. E.; Snaith, H. J.; McGehee, M. D. The renaissance of dye-sensitized solar cells. *Nat. Photonics* **2012**, *6*, 162–169.
- (21) Cheema, H.; Baumann, A.; Loya, E. K.; Brogdon, P.; McNamara, L. E.; Carpenter, C. A.; Hammer, N. I.; Mathew, S.; Risko, C.; Delcamp, J. H. Near-Infrared-Absorbing Indolizine-Porphyrin Push-Pull Dye for Dye-Sensitized Solar Cells. *ACS Appl. Mater. Interfaces* **2019**, *11*, 16474–16489.
- (22) Huckaba, A. J.; Giordano, F.; McNamara, L. E.; Dreux, K. M.; Hammer, N. I.; Tschumper, G. S.; Zakeeruddin, S. M.; Grätzel, M.; Nazeeruddin, M. K.; Delcamp, J. H. Indolizine-Based Donors as Organic Sensitizer Components for Dye-Sensitized Solar Cells. *Adv. Energy Mater.* **2015**, *5*, 1401629.
- (23) Brogdon, P.; Cheema, H.; Delcamp, J. H. Low-Recombination Thieno[3,4-b]thiophene-Based Photosensitizers for Dye-Sensitized Solar Cells with Panchromatic Photoresponses. *ChemSusChem* **2017**, *10*, 3624–3631.
- (24) Chen, Y. C.; Chou, H. H.; Tsai, M. C.; Chen, S. Y.; Lin, J. T.; Yao, C. F.; Chen, K. Thieno[3,4-b]thiophene-based organic dyes for dye-sensitized solar cells. *Chem.—Eur. J.* **2012**, *18*, 5430–5437.
- (25) Cheema, H.; Watson, J.; Peddapuram, A.; Delcamp, J. H. A 25 mA cm-2 dye-sensitized solar cell based on a near-infrared-absorbing organic dye and application of the device in SSM-DSCs. *Chem. Commun.* **2020**, *56*, 1741–1744.

- (26) Yu, Q.-Y.; Liao, J.-Y.; Zhou, S.-M.; Shen, Y.; Liu, J.-M.; Kuang, D.-B.; Su, C.-Y. Effect of Hydrocarbon Chain Length of Disubstituted Triphenyl-amine-Based Organic Dyes on Dye-Sensitized Solar Cells. *J. Phys. Chem. C* **2011**, *115*, 22002–22008.
- (27) Liu, J.; Zhou, D.; Xu, M.; Jing, X.; Wang, P. The structure-property relationship of organic dyes in mesoscopic titania solar cells: only one double-bond difference. *Energy Environ. Sci.* **2011**, *4*, 3545.
- (28) Liyanage, N. P.; Yella, A.; Nazeeruddin, M.; Grätzel, M.; Delcamp, J. H. Thieno[3,4-b]pyrazine as an Electron Deficient π -Bridge in D-A- π -A DSCs. ACS Appl. Mater. Interfaces **2016**, 8, 5376–5384.
- (29) Liyanage, N. P.; Cheema, H.; Baumann, A. R.; Zylstra, A. R.; Delcamp, J. H. Effect of Donor Strength and Bulk on Thieno[3,4-b]-pyrazine-Based Panchromatic Dyes in Dye-Sensitized Solar Cells. *ChemSusChem* **2017**, *10*, 2635–2641.
- (30) Watson, J.; Santaloci, T. J.; Cheema, H.; Fortenberry, R. C.; Delcamp, J. H. Full Visible Spectrum Panchromatic Triple Donor Dye for Dye-Sensitized Solar Cells. *J. Phys. Chem. C* **2020**, *124*, 25211–25220.
- (31) Paredes-Gil, K.; Páez-Hernández, D.; Arratia-Pérez, R.; Mendizábal, F. Insights into the role of D-A-π-A type pro-aromatic organic dyes with thieno[3,4-b]pyrazine as A acceptor group into dyesensitized solar-cells. A TD-DFT/periodic DFT study. *Int. J. Quantum Chem.* **2019**, *120*, No. e26108.
- (32) Huckaba, A. J.; Yella, A.; Brogdon, P.; Scott Murphy, J. S.; Nazeeruddin, M. K.; Grätzel, M.; Delcamp, J. H. A Low Recombination Rate Indolizine Sensitizer for Dye-Sensitized Solar Cells. *Chem. Commun.* **2016**, 52, 8424–8427.
- (33) Huckaba, A. J.; Yella, A.; McNamara, L. E.; Steen, A. E.; Murphy, J. S.; Carpenter, C. A.; Puneky, G. D.; Hammer, N. I.; Nazeeruddin, M. K.; Grätzel, M.; et al. Molecular Design Principles for Near-Infrared Absorbing and Emitting Indolizine Dyes. *Chem.—Eur. J.* **2016**, *22*, 15536–15542.
- (34) Li, P.; Zhang, H.; Troisi, A. Systematic Study of the Effect of Auxiliary Acceptors in D-A' $-\pi$ -A Sensitizers Used on Dye-Sensitized Solar Cells. *J. Phys. Chem. C* **2018**, *122*, 23890-23898.
- (35) Chou, H.-H.; Yang, C.-H.; Lin, J. T. s.; Hsu, C.-P. First-Principle Determination of Electronic Coupling and Prediction of Charge Recombination Rates in Dye-Sensitized Solar Cells. *J. Phys. Chem. C* 2016, 121, 983–992.
- (36) Kono, T.; Murakami, T. N.; Nishida, J.-i.; Yoshida, Y.; Hara, K.; Yamashita, Y. Synthesis and photo-electrochemical properties of novel thienopyrazine and quinoxaline derivatives, and their dye-sensitized solar cell performance. *Org. Electron.* **2012**, *13*, 3097–3101.
- (37) Lu, X.; Feng, Q.; Lan, T.; Zhou, G.; Wang, Z.-S. Molecular Engineering of Quinoxaline-Based Organic Sensitizers for Highly Efficient and Stable Dye-Sensitized Solar Cells. *Chem. Mater.* **2012**, 24, 3179–3187.
- (38) Lu, X.; Zhou, G.; Wang, H.; Feng, Q.; Wang, Z.-S. Near infrared thieno [3,4-b] pyrazine sensitizers for efficient quasi-solid-state dye-sensitized solar cells. *PCCP* **2012**, *14*, 4802–4809.
- (39) Tseng, C.-Y.; Taufany, F.; Nachimuthu, S.; Jiang, J.-C.; Liaw, D.-J. Design strategies of metal free-organic sensitizers for dye sensitized solar cells: Role of donor and acceptor monomers. *Org. Electron.* **2014**, *15*, 1205–1214.
- (40) Wu, J.; Li, G.; Zhang, L.; Zhou, G.; Wang, Z.-S. Energy level engineering of thieno[3,4-b]pyrazine based organic sensitizers for quasi-solid-state dye-sensitized solar cells. *J. Mater. Chem. A* **2016**, *4*, 3342–3355.
- (41) Brogdon, P.; Giordano, F.; Puneky, G. A.; Dass, A.; Zakeeruddin, S. M.; Nazeeruddin, M. K.; Grätzel, M.; Tschumper, G. S.; Delcamp, J. H. A Computational and Experimental Study of Thieno[3,4-b]thiophene as a Proaromatic π-Bridge in Dye-Sensitized Solar Cells. *Chem.—Eur. J.* **2016**, 22, 694–703.
- (42) Curiac, C.; Hunt, L. A.; Sabuj, M. A.; Li, Q.; Baumann, A.; Cheema, H.; Zhang, Y.; Rai, N.; Hammer, N. I.; Delcamp, J. H. Probing Interfacial Halogen-Bonding Effects with Halogenated Organic Dyes and a Lewis Base-Decorated Transition Metal-Based

Redox Shuttle at a Metal Oxide Interface in Dye-Sensitized Solar Cells. J. Phys. Chem. C 2021, 125, 17647–17659.

- (43) Kohlrausch, R. Theorie des elektrischen Rückstandes in der Leidener Flasche. Ann. Phys. 1854, 167, 179-214.
- (44) Lindsey, C. P.; Patterson, G. D. Detailed comparison of the Williams-Watts and Cole-Davidson functions. *J. Chem. Phys.* **1980**, *73*, 3348–3357.
- (45) Lukichev, A. Physical meaning of the stretched exponential Kohlrausch function. *Phys. Lett. A* **2019**, 383, 2983–2987.
- (46) Williams, G.; Watts, D. C. Non-Symmetrical Dielectric Relaxation Behaviour Arising from a Simple Empirical Decay Function. *Trans. Faraday Soc.* **1970**, *66*, 80–85.
- (47) Casarin, L.; Swords, W. B.; Caramori, S.; Bignozzi, C. A.; Meyer, G. J. Rapid Static Sensitizer Regeneration Enabled by Ion Pairing. *Inorg. Chem.* **2017**, *56*, 7324–7327.
- (48) DiMarco, B. N.; Troian-Gautier, L.; Sampaio, R. N.; Meyer, G. J. Dye-sensitized electron transfer from TiO2 to oxidized triphenylamines that follows first-order kinetics. *Chem. Sci.* **2018**, *9*, 940–949.
- (49) Becke, A. D. Density-functional thermochemistry. III. The role of exact exchange. *J. Chem. Phys.* **1993**, *98*, 5648–5652.
- (50) Lee, C.; Yang, W.; Parr, R. G. Development of the Colle-Salvetti correlation-energy formula into a functional of the electron density. *Phys. Rev. B: Condens. Matter Mater. Phys.* **1988**, 37, 785–789.
- (51) Frisch, M. J.; Pople, J. A.; Binkley, J. S. Self-consistent molecular orbital methods 25. Supplementary functions for Gaussian basis sets. *J. Chem. Phys.* **1983**, *80*, 3265–3269.
- (52) Frisch, M. J.; Trucks, G. W.; Schlegel, H. B.; Scuseria, G. E.; Robb, M. A.; Cheeseman, J. R.; Scalmani, G.; Barone, V.; Petersson, G. A.; Nakatsuji, H.; Li, X.; et al. *Gaussian 16*, Revision B.01; Gaussian, Inc.: Wallingford CT, 2016.
- (53) Helgaker, T.; Jaszuński, M.; Ruud, K. Ab Initio Methods for the Calculation of NMR Shielding and Indirect Spin-Spin Coupling Constants. *Chem. Rev.* **1999**, *99*, 293–352.
- (54) Ditchfield, R. Self-consistent perturbation theory of diamagnetism. *Mol. Phys.* **1974**, *27*, 789–807.
- (55) Sulas, D. B.; London, A. E.; Huang, L.; Xu, L.; Wu, Z.; Ng, T. N.; Wong, B. M.; Schlenker, C. W.; Azoulay, J. D.; Sfeir, M. Y. Preferential Charge Generation at Aggregate Sites in Narrow Band Gap Infrared Photoresponsive Polymer Semiconductors. *Adv. Optical Mater.* **2018**, *6*, 1701138.
- (56) Rosenberg, M.; Dahlstrand, C.; Kilså, K.; Ottosson, H. Excited state aromaticity and antiaromaticity: opportunities for photophysical and photochemical rationalizations. *Chem. Rev.* **2014**, *114*, 5379–5425.
- (57) Kotani, R.; Liu, L.; Kumar, P.; Kuramochi, H.; Tahara, T.; Liu, P.; Osuka, A.; Karadakov, P. B.; Saito, S. Controlling the S1 Energy Profile by Tuning Excited-State Aromaticity. *J. Am. Chem. Soc.* **2020**, 142, 14985.
- (58) Shokri, S.; Li, J.; Manna, M. K.; Wiederrecht, G. P.; Gosztola, D. J.; Ugrinov, A.; Jockusch, S.; Rogachev, A. Y.; Ayitou, A. J. A Naphtho-p-quinodimethane Exhibiting Baird's (Anti)Aromaticity, Broken Symmetry, and Attractive Photoluminescence. *J. Org. Chem.* **2017**, *82*, 10167–10173.
- (59) Lampkin, B. J.; Nguyen, Y. H.; Karadakov, P. B.; VanVeller, B. Demonstration of Baird's rule complementarity in the singlet state with implications for excited-state intramolecular proton transfer. *PCCP* **2019**, *21*, 11608–11614.
- (60) Tobe, Y. Quinodimethanes Incorporated in Non-Benzenoid Aromatic or Antiaromatic Frameworks. *Top. Curr. Chem.* **2018**, *376*, 12.

☐ Recommended by ACS

True- to Sky-Blue Emitters Bearing the Thiazolo [5,4-d]thiazole Electron Acceptor for Single and Tandem Organic Light-Emitting Diodes

Abdelaziz Jouaiti, Matteo Mauro, et al.

MAY 03, 2023

ACS APPLIED ELECTRONIC MATERIALS

READ 🗹

Accelerated Intramolecular Charge Transfer in Tetracyanobutadiene- and Expanded Tetracyanobutadiene-Incorporated Asymmetric Triphenylamine-Quinoxaline...

Youngwoo Jang, Francis D'Souza, et al.

MAY 16, 2023

THE JOURNAL OF PHYSICAL CHEMISTRY A

READ 🗹

Zero-Zero Energy-Dominated Degradation in Blue Organic Light-Emitting Diodes Employing Thermally Activated Delayed Fluorescence

Tiangeng Liu, Qisheng Zhang, et al.

MAY 05, 2022

ACS APPLIED MATERIALS & INTERFACES

READ 🗹

Finding New Precursors for Light Harvesting Materials: A Computational Study of the Fluorescence Potential of Benzanthrone Dyes

Yasir Altaf, Muhammad Ali Hashmi, et al.

NOVEMBER 17, 2021

ACS OMEGA

READ 🗹

Get More Suggestions >